Thouless energy as a unifying concept for Josephson junctions tuned through the Mott metal-insulator transition

A. N. Tahvildar-Zadeh and J. K. Freericks
Department of Physics, Georgetown University, Washington, DC 20057-0995, USA

B. K. Nikolić
Department of Physics and Astronomy, University of Delaware, Newark, Delaware 19716-2570, USA

(Received 2 September 2005; revised manuscript received 29 March 2006; published 12 May 2006)

The Thouless energy was introduced in the 1970s as a semiclassical energy for electrons diffusing through a finite-sized conductor. It turns out to be an important quantum-mechanical energy scale for many systems ranging from disordered metals to quantum chaos to quantum chromodynamics. In particular, it has been quite successful in describing the properties of Josephson junctions when the barrier is a diffusive normal-state metal. The Thouless energy concept can be generalized to insulating barriers by extracting an energy scale from the two-probe Kubo conductance of a strongly correlated electron system (metallic or insulating) via a generalized definition of the quantum-mechanical level spacing to many-body systems. This energy scale is known to determine the crossover from tunneling to Ohmic (thermally activated) transport in normal tunnel junctions. Here we use it to illustrate how the quasiclassical picture of transport in Josephson junctions is modified as the strongly correlated barrier passes through the Mott transition. Surprisingly, we find the quasiclassical form holds well beyond its putative realm of validity.

DOI: 10.1103/PhysRevB.73.184515 PACS number(s): 71.27.+a, 74.45.+c, 74.50.+r

I. INTRODUCTION

As the development and manufacture of Josephson devices is pushing toward nanoscales (submicron linear dimensions for the junction area and nanometer thicknesses for the barriers), it is natural to expect that the quasiclassical models will need improvements to have predictive power for short non-diffusive junctions (insulator barriers in the few nanometer range thickness) as well as long diffusive ones (metal barriers in the tens to hundreds of nanometer range thickness). Josephson junctions that are used as the primitive circuit elements for digital electronics employing rapid single flux quantum logic are required to be nonhysteretic. Conventional tunnel junctions are usually hysteretic, and need to be shunted by an additional resistor to have a single-valued current-voltage characteristic. Current focus on developing faster self-shunted Josephson junctions is searching for the optimal junction size and the optimal barrier material. This optimization can be addressed by using a microscopic model which properly deals with the atomic interfaces as well as the variation in carrier scattering strengths in the materials constructing the junction. It is our intent in this paper to show that the results of such a microscopic calculation agree well with and complement the predictions of the quasiclassical model for a wide range of parameters. To achieve this we need to express our results in terms of the Thouless energy which is the energy scale used in the transport problems of mesoscopic systems and is central to the quasiclassical analysis.

The Thouless energy scale was discovered by Thouless[1] in the 1970s while studying Anderson localization related problems: a heuristic analysis of the sensitivity of the energy levels in diffusive conductors to a change of boundary conditions pointed to the importance of the energy scale $E_{\mathrm{Th}} = \hbar \mathcal{D}/L_B^2$, where L_B is the thickness of the conductor and $\mathcal{D}$ is the diffusion constant for transport in the conductor. Although E_{Th} was introduced as the inverse of a purely classical time $L_B^2/\mathcal{D}$ (the dwell time in the conductor of thickness L_B), it is close to many *quantum-mechanical* energy scales[2] governing the physics of quasiparticles in disordered systems.[3] The Thouless energy has emerged as an essential energy scale in ballistic quantum dots,[4] quantum chaos,[5] quantum chromodynamics,[6] and mesoscopic superconductivity (including Josephson junctions).[7]

In the quasiclassical theory of Josephson junctions, it is known that the proximity-effect coupling of two superconductors through a noninteracting normal metal is governed by either the single-particle energy scale E_{Th} or the many-body superconducting gap Δ (whichever is smaller).[7,8] The physical picture is as follows: when a superconductor (S) with an essentially infinite phase coherence length is brought into proximity with a normal metal (N) with a long phase coherence length, the phase information is exchanged via the process of Andreev reflection[9] which kinematically correlates the phase of the two electrons (of a Cooper pair) as they leak from the S into the N. If a SNS junction is formed, with the thickness of the N layer being less than the phase-coherence length L_ϕ (determined by inelastic scattering processes), then quantum interference effects are possible for particles with energies smaller than E_{Th}. These low-energy particles are responsible for the experimental observation of long-range proximity effects[8] where single-particle properties (like anomalies in the density of states[10]) or kinetic quantities[11] in the N are affected on length scales $L_\omega = \sqrt{\hbar \mathcal{D}/2\omega} \gg \xi_N = \sqrt{\hbar \mathcal{D}/2\pi k_B T}$ for electrons with low energy $\omega \ll k_B T$. This can be contrasted with the traditional signature of the proximity effect,[12] due to thermal quasiparticles $\omega \simeq k_B T$ that vanish exponentially fast on length scales longer than ξ_N. For instance, the Josephson critical current in a SNS junction decays as $I_c \propto e^{-L_B/\xi_N}$ when the junction thickness L_B exceeds the normal metal coherence length ξ_N, due to the exponential decay of the pair-field amplitude in the N. On the

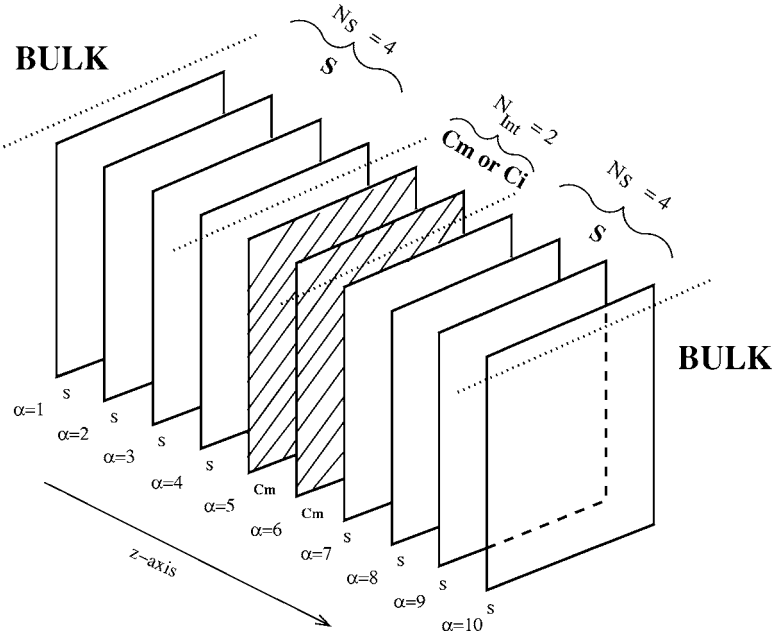

FIG. 1. Microscopic stacked planar geometry of a Josephson junction defined on an infinite simple cubic lattice with a lattice constant a. The barrier layers are correlated metal Cm (for $U^{\mathrm{FK}} < 4.9$) or correlated (Mott) insulator Ci (for $U^{\mathrm{FK}} \gtrsim 4.9$) described by the FK model, which is attached to two semi-infinite superconducting leads. These Cm or Ci planes, together with the first 30 superconducting planes in each lead, comprise the region of the junction where the self-consistent calculation is performed, while the rest of the infinite system is introduced via appropriate "boundary conditions." We consider barriers ranging in thickness from 1 to 200 planes.

other hand, examples of how the Thouless energy plays the role of the characteristic energy scale for proximity-induced superconductivity include the following: (i) the characteristic voltage (the product of I_c with the normal state resistance R_N) of a long diffusive *SNS* junction (with $E_{\mathrm{Th}} \ll \Delta$) is determined by a universal function of the Thouless energy[7] (which approaches $I_c R_N \sim 10.82 E_{\mathrm{Th}}$ at zero temperature), whereas in short junctions (with $\Delta \ll E_{\mathrm{Th}}$) it is determined by the superconducting gap[13] $I_c R_N \sim 0.66\pi\Delta/e$; (ii) a minigap $\sim E_{\mathrm{Th}}$ opens in the density of states (DOS) of a disordered or ballistic chaotic Fermi liquid N in a "closed" geometry;[10] (iii) the conductance of a proximity-coupled N exhibits a non-monotonic temperature and voltage dependence with a maximum occurring when[10,14] $k_B T$ or $eV \approx E_{\mathrm{Th}}$. In this paper, we use the generalized definition for the Thouless energy[15] [which includes non-diffusive junctions with a correlated metal (Cm) or correlated insulator (Ci) as the barrier] to study the characteristic voltage of such junctions and compare the results with those of quasiclassical models. A short communication on these results with a focus toward applications has already appeared.[16]

In Sec. II, we describe the model and the formalism. In Sec. III, we introduce the important energy scales of the Josephson junction, while in Sec IV, we do the same for length scales. Section V discusses the relation to Friedel oscillations and Sec. VI provides the conclusions.

II. MODEL AND METHODS

The formalism for calculating properties of Josephson junctions with strongly correlated barriers has been developed[17] by employing inhomogeneous dynamical mean-field theory (DMFT).[18] We have an algorithm to compute the conductance of a finite thickness slab of correlated material attached to two leads, and to determine the critical current at zero voltage. This is all that is needed to produce the figure-of-merit $I_c R_N$ for Josephson junctions. The geometry of our multilayered nanostructure is shown schematically in Fig. 1 and is the standard two-probe measurement configuration used in mesoscopic physics,[3] except that the cross sections of both the leads and the sample are infinite. We choose to model the barrier by a Falicov-Kimball (FK) model,[19] where increasing the local Coulomb interaction drives the system from a non-Fermi liquid phase toward a critical metal, and eventually into a (Mott) correlated insulator. Besides being tunable through the Mott transition, the FK model is the simplest many-body model that includes the scattering of charge carriers off static ions which make it suitable to model diffusive as well as insulating barriers. Indeed, the charge fluctuations that yield the strongly correlated insulator are identical for the FK model and the Hubbard model in the appropriate configurations; in the FK model, exactly two conduction electrons per sites with no impurity ion and no electrons on sites occupied by impurity ions, and in Hubbard model, exactly one conduction electron per site. This mapping between the two requires us to first note that the spin dependence of the spin one-half FK model is trivial, so we can just as well consider a spinless FK model with one conduction electron on the sites with no impurities. Then, if we identify the conduction electrons with the spin-up electrons and the impurity ions with the spin down electrons we have the Hubbard model, except the down spin electrons now do not hop. The main difference between the solutions of the two models is on the metallic side where the FK model is not a Fermi liquid.

The Josephson junction is then described by the Hamiltonian

$$\hat{\mathcal{H}} = -\sum_{ij\sigma} t_{ij} c_{i\sigma}^{\dagger} c_{j\sigma} + \sum_i U_i^H \left(c_{i\uparrow}^{\dagger} c_{i\uparrow} - \frac{1}{2} \right) \left(c_{i\downarrow}^{\dagger} c_{i\downarrow} - \frac{1}{2} \right) + \sum_{i\sigma} U_i^{\mathrm{FK}} c_{i\sigma}^{\dagger} c_{i\sigma} \left(w_i - \frac{1}{2} \right), \tag{1}$$

of interacting electrons that live on an infinite set of stacked

square lattice planes, depicted in Fig. 1, whose connectivity is the same as a simple cubic lattice (with lattice constant a). Here $c^{\dagger}_{i\sigma}$ ($c_{i\sigma}$) creates (destroys) an electron of spin σ at site i, $t_{ij}=t$ (the energy unit) is the hopping integral between nearest-neighbor sites i and j (chosen to be the same within the planes and between planes), U^H_i is the attractive Hubbard interaction for sites within the superconducting planes, U^{FK}_i is the FK interaction for planes within the barrier region, and w_i is a classical variable that equals 1 if an A ion occupies site i and is zero if a B ion occupies site i. The chemical potential μ is set equal to zero to yield half filling of the conduction electrons in all layers of the device. We also choose the average concentration of the scatterers in the barrier to be 1/2. One can view the strong correlations in the barrier in a binary alloy picture containing itinerant electrons and immobile A and B ions at 50% concentration, with U^{FK} being the difference in site energy between the A and B ionic sites.

The many-body problem is solved by taking an annealed average that yields essentially the coherent potential approximation. By employing DMFT, the exact solution of the FK model can be obtained in the infinite-dimensional limit, offering the simplest ground for testing new ideas in strongly correlated physics.[20] In this study we used a simple cubic three-dimensional bare DOS in the DMFT algorithm to obtain the local Green functions. In the bulk, the FK correlated metal undergoes a MIT at $U^{\mathrm{FK}}\approx 4.9t$. Since the system is not a Fermi liquid for nonzero U^{FK}, the DOS first develops a pseudogap, and then is suppressed entirely to zero in a continuous fashion, as the correlations increase and the system eventually becomes a correlated insulator.

The equilibrium superconducting state properties of the SCmS Josephson junction are computed by employing the Nambu-Gor'kov matrix formulation for Green functions with a local self-energy. The attractive Hubbard interaction is treated in the Hartree-Fock approximation, which generates a BCS superconductor in the S leads. In this approximation the matrix Green function satisfies a modified version of the Bogoliubov-de Gennes equation (due to a non-zero U^{FK}). We exploit translational invariance within the planes perpendicular to the supercurrent direction to perform a Fourier transform over the planar coordinates and reduce the problem to a one spatial dimension equation for the 2×2 matrix Green function $\mathbf{G}_{\alpha,\beta}$ between planes (the formalism is discussed in Refs. 17 and 15). We solve these equations self-consistently by using inhomogeneous DMFT.[18]

To calculate the superconducting pair-field Green's function on each plane (F_α) we need to compute the local off-diagonal Matsubara frequency Green function since $F_\alpha = 2T\Sigma_n \mathbf{G}^{12}_{\alpha,\alpha}(i\omega_n)$ where $\omega_n=(2n+1)\pi k_b T$ is the Fermionic Matsubara frequency (note that the superconducting gap is $\Delta_\alpha = U^H_\alpha F_\alpha$). Throughout this study we choose $U^H_i=-2t$ and $U^{FK}_i=0$ in the leads, yielding a transition temperature $T_c=0.11t$ for the leads, with the corresponding zero-temperature superconducting gap $\Delta=0.198t$. Also for definiteness we choose $U^H_i=0$ in the barrier so that the superconducting gap $\Delta=0$ in that region although the pair-field Green's function F is generally nonzero due to the proximity effect (Andreev reflection). This effect also causes the pair-field Green's function in the superconducting leads to decay as we approach the SN interface. Figure 2 shows the spatial dependence of the pair-field Green's function in the left half of the junction (symmetric for the other half) for $T=0.09T_c$ and two different values of U^{FK}. The Josephson junction has 30 self-consistent S planes to the right and to the left and 20 planes in the barrier. The barrier is insulating for $U^{\mathrm{FK}}=6$ and is a strongly scattering diffusive metal for $U^{\mathrm{FK}}=2$.

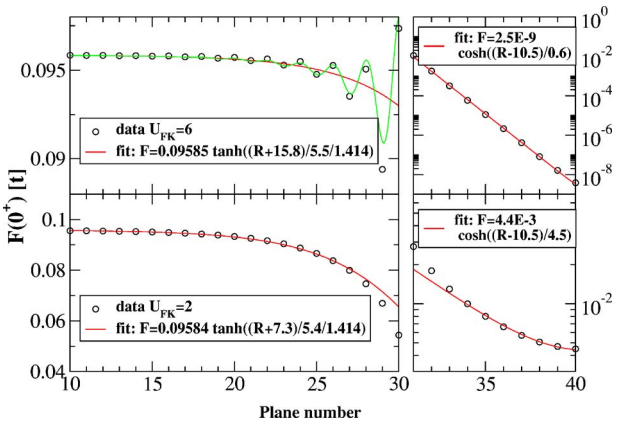

FIG. 2. (Color online) Pair-field Green's function $F(z)$ for half of the junction (F is symmetric about 40.5 for the other half). For clarity the scales are chosen to be different in the lead and barrier regions. Circles and lines represent the calculated data and the fits, respectively. In the barrier $U^{\mathrm{FK}}=2t$ for the lower half and $U^{\mathrm{FK}}=6t$ for the upper half. R stands for the distance from interface $|x-30.5|$.

Note how the pair-field amplitude behaves in these two different cases. When the barrier is insulating ($U^{\mathrm{FK}}=6$), the pair-field amplitude has both oscillatory behavior and a decay as the barrier is approached from the lead, while in the metallic barrier ($U^{\mathrm{FK}}=2$), the oscillations are greatly suppressed. The decay in the barrier is clearly exponential in the insulator, but is much less rapid in the metal. The numerical data are indicated by the symbols, while the lines are various fits that include or ignore the oscillations, as described in the following. Note that we have carefully checked the numerical convergence of both the quadratures and the iterations to verify that these oscillations are real and not an artifact of poor numerics.

The supercurrent is computed from the nearest-neighbor diagonal Green function:

$$I^s_{\alpha,\alpha+1} = A\left(\frac{4eta}{\hbar}\right) T\sum_n \mathbf{G}^{11}_{\alpha,\alpha+1}(i\omega_n), \tag{2}$$

where A is the junction area normal to the current direction. The pair-field amplitude is a complex quantity $F_\alpha=|F_\alpha|e^{i\phi_\alpha}$ bearing the condensate phase on each plane. There must be a phase difference across the junction in order to sustain a supercurrent. In the case of a bulk superconductor with no barrier, the phase profile is linear $\phi_\alpha=qa\alpha$. For an SCmS Josephson junction, the phase profile is more complicated and must be determined self-consistently. In the presence of current, the translational invariance is broken in the direction of the current and unlike the zero current case, the

Bogoliubov-de Gennes equations cannot be diagonalized by simple Fourier transformation to momentum space ($\mathbf{G}_{\alpha,\beta}$ is not a function of $z_\alpha - z_\beta$ alone). We overcome this problem by making a canonical transformation of the electron creation and annihilation operators, $c_{\alpha\sigma}=\exp[-i\Phi_\alpha/2]\hat{c}_{\alpha\sigma}$, at each self-consistency step, where Φ_α is the total phase accumulated by F_α. This transformation renders each F_α real, but distributes their (accumulated) phases onto the transformed hopping matrix elements $\hat{t}_{\alpha,\alpha+1}=\exp[i(\Phi_{\alpha+1}-\Phi_\alpha)/2]t_{\alpha,\alpha+1}$. Moreover, to get a finite current, we apply a boundary condition that locks the phase gradient between the bulk and the first plane of the left superconducting lead to a constant q at each self-consistency iteration. In this fashion, we match the incident supercurrent to that of the bulk lead with a phase gradient of q. Hence, our computational procedure works with current-biased junctions, just like in experiment. Our calculations fail, due to numerical precision, when the critical current through the junction becomes too small to be handled with double precision arithmetic (approximately $10^{-12}I_c^{\mathrm{Bulk}}$), but we can describe all physically interesting systems without any numerical issues.

Figure 3 shows the critical current in the junction versus the barrier thickness. The critical current density I_c/A is determined by gradually increasing the total phase difference accumulated by the pair-field amplitude throughout the junction (by increasing q at the first plane). Then we measure the total phase difference across the barrier $\Delta\phi$ (by accumulating the phase differences across each barrier plane) and we measure the current density passing through the junction by directly evaluating the current passing from one plane to its neighbor (current conservation guarantees that this measurement can be done at any plane and indeed our self-consistent calculations do obey current conservation). Finally, we repeat this exercise until the supercurrent reaches a maximum as shown in the inset to Fig. 3 for the case of a ballistic barrier ($U^{\mathrm{FK}}=U^H=0$). The critical current density of the bulk superconductor I_c^{Bulk}/A is calculated similarly by increasing the phase gradient in the bulk until the current is maximized. For the parameters chosen in this paper, we find $I_c^{\mathrm{Bulk}}/A=0.014(4et/ha^2)$. We observe that except for very thin junctions, I_c is an exponentially decreasing function of the thickness in accordance with phenomenological theories.[21] The rate of decrease increases dramatically as the barrier goes from being a metal to being an insulator.

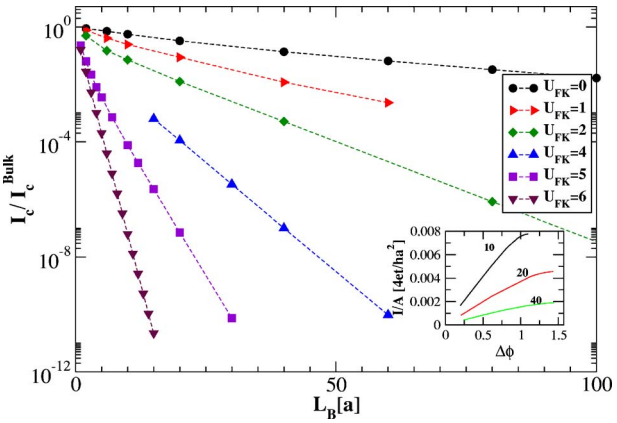

FIG. 3. (Color online) Relative critical current of the junction versus its thickness for different values of scattering strength in the barrier for $T=0.01t$. The bulk value is $I_c^{\mathrm{Bulk}}/A=0.014(4et/ha^2)$. The inset shows supercurrent versus phase difference across a ballistic barrier for thicknesses of $10a$, $20a$, and $40a$.

To calculate the normal state resistance R_N, our setup in Fig. 1 corresponds to a slab of the Cm which is attached to two clean normal metal leads; the analytically continued Green function $G_{\alpha,\beta}(\omega+i0^+)$ makes it possible to obtain the dc Kubo resistance[15] from the particle-hole bubble with no vertex corrections[22] (technically speaking the vertex corrections need not vanish in inhomogeneous DMFT, but because they are expected to be small since they arise from the electron-electron interaction, we neglect them in our analysis):

$$R_N A = \sum_{\alpha\beta} \sigma_{\alpha\beta}^{-1},$$

$$\sigma_{\alpha\beta} = \frac{e^2a^4t^2}{2hk_BT}\int_{-\infty}^{\infty} d\omega \int_{-\infty}^{\infty} d\epsilon \rho^{2d}(\epsilon) \frac{\mathrm{Im}\, G_{\alpha,\beta+1}(\epsilon,\omega)\mathrm{Im}\, G_{\beta,\alpha+1}(\epsilon,\omega) - \mathrm{Im}\, G_{\alpha,\beta}(\epsilon,\omega)\, \mathrm{Im}\, G_{\beta+1,\alpha+1}(\epsilon,\omega)}{\cosh^2(\omega/2k_BT)}, \tag{3}$$

where the inverse is taken as a matrix inverse. Figure 4 shows the normal-state resistance of the barrier times the junction area versus its thickness for $T=0.01t$. Note that the scaling of the resistance with the finite thickness L_B (of the slab of strongly correlated material) is linear in the Cm phase all the way to the MIT; in the Ci phase, it typically has exponential growth with the thickness in the tunneling regime, which gives way to linear growth (with a strongly temperature-dependent slope) after the crossover to thermally activated transport.[15] Notice how for $U^{\mathrm{FK}}=6$ the normal-state resistance begins to deviate from exponential growth for larger values of the thickness (see the inset of Fig. 4 which depicts R_N for $U^{\mathrm{FK}}=6$ at a higher temperature $T=0.1t$); R_N first increases exponentially with L_B, but then crosses over to the linear regime for $L_B>5a$ (at this temperature). Hence in the insulating regime of the FK model, which has a gap at E_F, tunneling is the preferred conduction mechanism at low T (R_N depends exponentially on L_B), but as T is

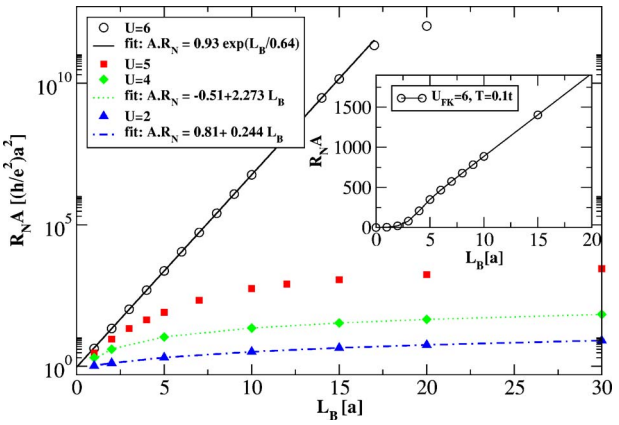

FIG. 4. (Color online) Normal-state resistance times junction area versus barrier length L_B. A is the junction area. The fits suggest that R_N is linear in size for $U^{\mathrm{FK}}<5$ and exponential for $U^{\mathrm{FK}}>5$ up to some length scale (called the Thouless length).

increased, incoherent thermal processes for conduction (i.e., diffusion) eventually become dominant and R_N becomes Ohmic (R_N depends linearly on L_B).[15]

III. ENERGY SCALES

In the following we explore the relevant energy scales for transport in the nanostructure. We measure the energies in units of the hopping integral t in our model. The electronic structure bandwidth for the tight-binding part of the model is $12t$, hence for typical materials of interest (e.g., Ta, Nb, and their nitrides) with bandwidths of 3–4 eV we get $t \sim 0.25$–0.33 eV. The operating temperature is set to $T=0.01t$ in this work unless otherwise stated. As mentioned before for the Hubbard interaction chosen here the zero temperature superconducting gap is $\Delta(0)=0.198t$ corresponding to $T_c=0.11t$; i.e., this is a high-temperature, short-coherence-length s-wave superconductor.

A. Thouless energy

Since the concept of a Thouless energy has had such success in describing the transport properties of quasiparticles, one can ask the question: *Is there an energy scale that provides similar guidance for transport when the (dirty) Fermi liquid N is replaced by a strongly correlated material*? The answer is yes, and we now describe how this can be done. We begin with the dimensionless conductance $g=G/G_Q$ with $G_Q=2e^2/h$ being the quantum unit of conductance. In Fermi-liquid systems, one can express the dimensionless conductance of a finite-size Fermi-liquid system as the ratio of the Thouless energy to the average quantum-mechanical level spacing[3,23] Δ_E,

$$g = 2\pi \frac{E_{\mathrm{Th}}}{\Delta_E}. \tag{4}$$

This relation was used to analyze the Anderson localization-delocalization transition, which occurs at $g\sim 1 \Leftrightarrow E_{\mathrm{Th}} = \mathcal{O}(\Delta_E)$, in terms of the relevant energy scales.[3] Inspired by Eq. (4), which interprets the dimensionless conductance as the Thouless energy (a transport energy scale) measured in the units of Δ_E (a thermodynamic energy scale), we propose a generalization of the Thouless energy to strongly correlated systems:

$$E_{\mathrm{Th}} = \frac{G_N}{2\pi G_Q \Omega \int d\omega N(\omega)[-\partial f/\partial\omega]}, \tag{5}$$

which extracts the relevant energy scale from the (normal-state) two-probe conductance $G_N=1/R_N$ of a strongly correlated sample of volume Ω. The key development in this analysis is the numerical extraction of the two-probe conductance of a strongly correlated material of finite thickness sandwiched between two ideal semi-infinite metal leads by using inhomogeneous DMFT.[15] The integral in the denominator is our definition of the inverse 'mean level spacing' $\Delta_E^{-1} \equiv \Omega(\partial n/\partial\mu)$, where $n=\int d\omega N(\omega) f(\omega-\mu)$ is the thermodynamic average concentration of electrons (per spin), μ is the chemical potential, and $f(\omega-\mu)=1/[1+\exp(\{\omega-\mu\}/k_BT)]$ is the Fermi-Dirac distribution function. The bulk DOS $N(\omega)$ (per spin) is related to the imaginary part of the local single-particle Green function $N(\omega)=-\mathrm{Im}G_{\mathrm{loc}}(\omega+i0^+)/\pi$ for strongly correlated electrons. For a metal at low temperature, the formula in Eq. (5) reduces to $E_{\mathrm{Th}} \approx G_N/2\pi G_Q \Omega N(\mu)$, which is the conventional result for diffusive systems.

The expression for the Thouless energy in Eq. (5) agrees with the usual results in the appropriate limits. To begin, recall that the DOS for a noninteracting metal, with a dispersion $\epsilon_k=\hbar^2k^2/2m$, satisfies $N(\mu)=2mk_F/h^2$, and the Fermi velocity satisfies $v_F=d\epsilon_k/dk\hbar=\hbar k_F/m$ with k_F the Fermi wave vector and m the effective mass of the quasiparticle. Next, note that the Drude form for the conductivity is $\sigma=k_F^2\ell G_Q/3\pi$ (with ℓ the mean free path) which can be used to extract a diffusion constant via the Einstein relation $\sigma=2e^2\mathcal{D}N(\mu)$. This then yields $\mathcal{D}=v_F\ell/3$ and $E_{\mathrm{Th}}=\hbar\mathcal{D}/L_B^2$, as expected. For a ballistic metal junction, with a transmissivity $\mathcal{T}$ at the lead-metal interface, we find the conductance is given by $g=k_F^2A\mathcal{T}/4\pi$ with A the cross-sectional area of the sample. Using the inverse level spacing Δ_E^{-1} for a sample of thickness L_B, $\Delta_E^{-1}=AL_B2mk_F/h^2$, then yields $E_{\mathrm{Th}}=\hbar v_F\mathcal{T}/4L_B$, which is the expected form. Note, however, that if we use the actual numerical conductance for a diffusive sample attached to metallic leads, the conductance includes the sum of both a contact resistance and the diffusive contributions from the "bulk" of the barrier region;[15] hence, Eq. (5) properly interpolates between the ballistic and diffusive limits, without needing to introduce a diffusion constant, or determine *a priori* whether the transport is ballistic or diffusive.

Note, however, that when we use Eq. (5) to describe the Thouless energy of correlated insulators, we find that the Thouless energy picks up significant temperature dependence because the conductance of a finite-thickness slab is finite at $T=0$ due to tunneling, but the average level spacing approaches infinity (due to the gap in the DOS), so the Thouless energy diverges as $T\to 0$. We find that the condition $E_{\mathrm{Th}}(T)\approx k_BT$ determines many of the crossovers from quantum to thermally activated behavior.[15] This is because once

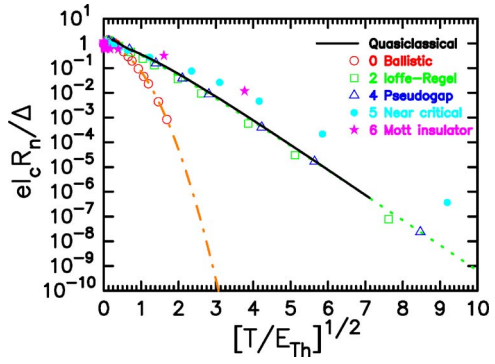

FIG. 5. (Color online) Characteristic voltage I_cR_N of SCmS and SCiS Josephson junctions; the temperature satisfies $k_BT=0.01$. The case $U^{FK}=0$ is a ballistic case, which follows the expected exponential curve given by the chain-dotted line. The case $U^{FK}=2$ is close to the Ioffe-Regel limit, where the mean-free-path approaches a lattice spacing, while the case $U^{FK}=4$ is an anomalous metal (the dotted line is a guide to the eye), whose resistance decreases as T increases due to the development of a depletion of DOS near the Fermi level (pseudogap) from the strong correlations. Nevertheless, both of these diffusive metals fall onto the universal quasiclassical prediction of Ref. 7 (solid line). Once we move into insulating barriers $U^{FK}=5$ (near the critical value of the metal-insulator transition) and $U^{FK}=6$ (a small-gap Mott insulator), we find that the deviations from the quasiclassical curve increase.

E_{Th} becomes smaller than the average level spacing, we expect thermal activation to govern the transport through the device, as shown in the general relation between the Thouless energy and the conductance in Eq. (4).

B. Figure of merit I_cR_N

We now examine the role of the Thouless energy in a more complex quantum phenomenon, namely Cooper pair tunneling in nanostructures. In general, the figure-of-merit will decrease as the barrier is made thicker. This is because the critical current decreases exponentially with the thickness, while the normal-state resistance is (i) independent of thickness for a ballistic metal, (ii) depends linearly on thickness for a diffusive metal, or (iii) depends exponentially on thickness crossing over to a linear dependence on thickness for insulators. Hence the critical current is expected to always decrease faster than the resistance increases, leading to a drop in the figure-of-merit as the barrier is made thicker. Unfortunately, from a manufacturing standpoint, thicker barriers are preferred, because they are more likely not to have defects or "pinholes" in them. One of the goals of the optimization process is to find the thickest barriers that still have acceptable figures-of-merit.

In Fig. 5, we plot the characteristic voltage of a Josephson junction, with the barrier described by a correlated metal or correlated insulator (determined by the interaction strength U^{FK}), versus $\sqrt{T/E_{Th}}$ where E_{Th} is the generalized Thouless energy. Since $E_{Th}=\hbar\mathcal{D}/L_B^2=2\pi k_BT\xi_T^2/L_B^2$ for a diffusive metal (where ξ_T is the thermal diffusion length) the horizontal axis of this figure is just L_B/ξ_T times a constant for diffusive barrier junctions. We include theoretical plots of the expected form for a ballistic *SNS* junction (where the critical current decreases exponentially with thickness, but the resistance is independent of thickness), and the quasiclassical formula from Ref. 7 evaluated at the temperature $T/T_c=1/11$. Note how all diffusive metals obey the quasiclassical prediction, even when we are well beyond the Ioffe-Regel limit[24] ($\ell\approx 2.3a$ for $U^{FK}=2$ and $\ell\approx 0.24a$ for $U^{FK}=4$). As the barrier goes through a Mott transition, we see the quasiclassical approach breaks down, overestimating the characteristic voltage for large E_{Th} and underestimating for small E_{Th}, with the crossover occurring at $E_{Th}\approx 0.01$. Note that the correlated insulators may have a universal form different from the quasiclassical one for small E_{Th}, since the $U^{FK}=5$ and 6 data lie close to each other. We are unable to generate enough data to see if a universal form is appropriate or if the above result is just a coincidence. One might expect universality, since at high temperatures, or for thick barriers, where the transport is thermally activated and diffusive, a quasiclassical picture might apply; our analysis shows that if this is so, the universal curve is modified from the conventional quasiclassical approach. These results show that the generalized form for the Thouless energy properly describes the quantum-mechanical phase coherence of the proximity effect in both correlated metals and correlated insulators.

One can also plot the figure-of-merit versus the Thouless energy directly and see how the Ci junctions begin to deviate from the quasiclassical form. The results[16] are similar to our above approach, and show once again that the quasiclassical form extends far beyond its putative region of validity to describe devices with mean free paths much smaller than a lattice spacing. It even gets the general qualitative behavior (and even a semiquantitative behavior) for the correlated insulator correct. We expect that there will be other examples of where this generalized Thouless energy will be the important energy scale to describe quantum-mechanical phenomena in strongly correlated systems.

IV. LENGTH SCALES

In this section we want to explore the various length scales for our nanostructure model that are relevant to charge transport across the junction. Unless stated otherwise their values are reported for an operating temperature of $T=0.01t=0.09T_c$ and the lengths are measured in units of the lattice constant a.

A. Superconducting and normal coherence lengths

We can quantify the decay of the superconducting pair-field amplitude F near the interfaces by fitting our data in Fig. 2 to the following form:

$$F(x)=\begin{cases} F_\infty \tanh\left(\dfrac{x+x_0}{\sqrt{2}\xi_{GL}}\right) & \text{inside the lead} \\ F_c \cosh\left(\dfrac{x}{\xi_N}\right) & \text{inside the barrier,} \end{cases} \tag{6}$$

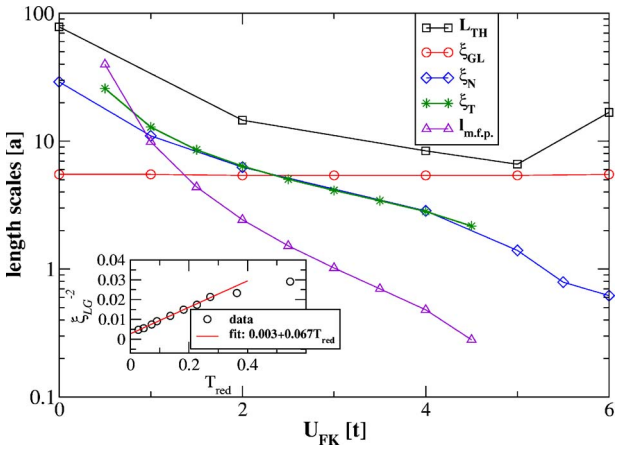

FIG. 6. (Color online) Length scales for Josephson junctions. These length scales are extracted by examining the fits of different measurable quantities to the thickness of the barrier for various values of the interaction strength U^{FK}, as described in the text. The Ginsburg-Landau length scale (circles with black line) is independent of the interaction strength, since it depends solely on the properties of the superconducting leads. The Thouless length (squares with red line) shows the thickness at which the tunneling/Ohmic crossover occurs in the transport in the correlated insulator. It is not clear how to interpret it in the diffusive metal. The normal-metal coherence length (diamonds with green line) agrees with the diffusion length (closed diamonds with blue line) when the barrier is a diffusive metal. Finally, the mean-free-path (triangles with magenta line) is the smallest length scale, and falls below the lattice constant when $U^{\mathrm{FK}} \approx 3t$. Inset is a plot of the temperature dependence of the inverse square of the Ginsburg-Landau length scale as T_c is approached, which shows the expected linear behavior.

where x is the distance from the center of the junction and F_∞, F_c, x_0, ξ_N, and ξ_{GL} are phenomenological parameters that are determined from the fit. The tanh form in the leads is inspired by the Ginsburg-Landau phenomenological theory[25] for an *SN* interface when T is near T_c. The cosh form in the barrier is the simplest smooth even function which has exponential decay near the interfaces, *although this function is not a solution to the Ginsburg-Landau equation*. For larger values of U^{FK} the order parameter in the leads has an oscillatory spatial dependence as is evident from the top portion of Fig. 2. We will argue in a later section that this oscillatory behavior is analogous to Friedel oscillations in the charge density in the presence of interfaces and in order to take it into account we use a sinus-modulated form of Eq. (6) for fitting $U^{\mathrm{FK}} > 3$ data.

Here we are mainly interested in estimating the values of coherence lengths ξ_N and ξ_{GL} (which are practically independent of the Friedel oscillation parameters). In order to reduce the number of fitting parameters for the lead, we first estimate the value of F_∞ by performing a self-consistent bulk calculation for the superconducting order parameter, then we use a least-squares fitting routine to fit the values of F at the first 25 planes of the lead to estimate x_0 and ξ_{GL}. The results are shown in Fig. 6 along with other length scales for the nanostructure operating at $T=0.09T_c$ for various values of U^{FK}. We believe that the reported values for ξ_N and ξ_{GL} are accurate to within a few percent. We see that the value of $\xi_{\mathrm{GL}} \approx 5a$ independent of the scattering strength in the barrier, which is natural since this is a length scale for the superconducting order parameter and should not depend on the details of scattering in the barrier.

According to the Ginsburg-Landau theory this order parameter healing length scale is related to the intrinsic coherence length ξ_0 near the transition temperature by $\xi_{\mathrm{GL}}(T) = 0.74\xi_0 T_{\mathrm{red}}^{-1/2}$ for a pure metal, and $\xi_{\mathrm{GL}}(T) = 0.85\sqrt{\xi_0 \ell} T_{\mathrm{red}}^{-1/2}$ for a dirty metal, where $T_{\mathrm{red}} = (1 - T/T_c)$ and ℓ is the mean-free-path.[25] Since we assume no scattering inside the superconducting lead we can estimate ξ_0 by studying the order parameter near T_c and applying the above formula for the case of pure metals. The inset to Fig. 6 suggests that $\xi_{\mathrm{GL}}(T)$ indeed scales like $(1 - T/T_c)^{-1/2}$ near T_c and the slope of the line suggests a value of $\xi_0 \approx 5.2a$.

An independent way to cross check this value is by using the BCS expression $\xi_0 = \hbar v_F / \pi\Delta(0)$ where v_F is the average electron velocity over the Fermi surface and $\Delta(0)$ is the pair potential at $T=0$. We estimate v_F by its value for a tight-binding model [the Hamiltonian in Eq. (1) with $U^{\mathrm{FK}} = U_H = 0$] where the band dispersion is $\epsilon_{\mathbf{k}} = -2t\Sigma_{i=1}^{3} \cos(\mathbf{k}_i a)$. Since $\hbar \mathbf{v}_{\mathbf{k}} = -\nabla_{\mathbf{k}} \epsilon_{\mathbf{k}}$ and at half-filling $\epsilon_F = 0$ we get

$$\hbar v_F = \frac{\int_{FS} da |\hbar\, \mathbf{v}_{\mathbf{k}}|}{\int_{FS} da} = \frac{\int d^3k \delta(\epsilon_{\mathbf{k}} - \epsilon_F) |\nabla_{\mathbf{k}} \epsilon_{\mathbf{k}}|^2}{\int d^3k \delta(\epsilon_{\mathbf{k}} - \epsilon_F) |\nabla_{\mathbf{k}} \epsilon_{\mathbf{k}}|}, \tag{7}$$

where the $\mathbf{k}$ integrals are over the first Brillouin zone. In order to numerically calculate the $\mathbf{k}$ integrals, we express the delta functions as

$$\delta(\epsilon_{\mathbf{k}} - \epsilon_F) = -\frac{1}{\pi} \mathrm{Im}\left(\frac{1}{\epsilon_{\mathbf{k}} - \epsilon_F + i0^+} \right) \tag{8}$$

and estimate the integrals by sums over a $(300)^3$ mesh of the first Brillouin zone. Our estimate for the average Fermi velocity is $v_F \approx 3.15at/\hbar$. In our model $\Delta(0) = 0.198t$, hence we get $\xi_0 \approx 5.1a$ which agrees well with our previous calculation.

Unlike the superconducting coherence length, the normal metal decay length $\xi_N(L_B)$, determined by the exponential decay of the pair-field amplitude in the barrier, is an increasing function of the barrier width for thin junctions, but it approaches a maximum value as the junction becomes thicker. We identify this limit as the normal metal coherence length scale ξ_N. It is also found to be a decreasing function of the scattering strength U^{FK}. This makes physical sense, since we believe the nonzero pair-field amplitude in a metallic barrier is due to the Andreev reflection mechanism, so the larger the scattering strength in the barrier, the closer to the interface that the electron-hole pairs dissociate. Although this length scale is found in the absence of any current passing through the structure, we will see in following that it also governs the decrease of supercurrent with the barrier width of the junction.

B. Critical current and thermal diffusion lengths

From Fig. 3, it is evident that the critical current decreases exponentially with the barrier thickness. The corresponding decay length $\xi_{I_c}(U^{\mathrm{FK}})$ can be measured from the slope of the lines on a log-linear plot. We find that this length scale coincides with the normal metal coherence length extracted from the decay of the pair-field amplitude in the barrier as outlined in the previous section, i.e., $\xi_{I_c}(U^{\mathrm{FK}})=\xi_N(U^{\mathrm{FK}})$. This is a non-trivial result of our calculations, since it shows that two apparently different length scales extracted from two different quantities (F versus I_c) at two different conditions (no current versus critical current in the junction) numerically coincide at each U^{FK}. Hereafter, we denote both of these length scales by ξ_N.

In Fig. 6, we see that ξ_N decreases significantly with increasing U^{FK} suggesting that this length scale, unlike ξ_{GL}, depends strongly on the conduction mechanism in the barrier. In fact, when we calculate the thermal diffusion length $\xi_T=\sqrt{\hbar\mathcal{D}/2\pi k_B T}$, it coincides with the value of ξ_{I_c} for diffusive barriers ($1<U^{\mathrm{FK}}<4.5$) as is apparent from Fig. 3, and in accordance with phenomenological theories of weak links.[21] We calculate $\mathcal{D}$ by using the Einstein relation $\sigma=2e^2N(\mu)\mathcal{D}$ and a bulk calculation for the electrical conductivity σ (which also coincides with the conductivity extracted from the slope of the linear fits to the normal state resistance in Fig. 4). We use the same formula for diffusive metals as for correlated insulators, so the data for $U^{\mathrm{FK}}>5$ may not have a true physical meaning when the barrier has its transport dominated by tunneling.

C. Mean free path

In a diffusive metal the mean free path and diffusion constant are related by $\mathcal{D}=v_F\ell/3$. We use our previously mentioned estimates of $\mathcal{D}$ and v_F to calculate ℓ. This procedure is certainly valid for all correlated metals since they do have diffusive transport and the diffusion constant is well defined (even for mean free paths less than a lattice spacing). We continue to use it for the correlated insulators, but there the procedure may be flawed and the concept of a mean-free-path may no longer be valid. As shown in Fig. 6 the mean free path decreases sharply with increasing the scattering strength in the barrier. Note that the Ioffe-Regel limit ($\ell\sim a$) occurs for $U^{\mathrm{FK}}\sim 3t$ but as seen in Fig. 4 the normal state resistance still looks like that of a diffusive metal (Ohmic) well beyond this limit for $U^{\mathrm{FK}}=4t$. In the Falicov-Kimball model, the mean-free path continuously goes to zero at the metal-insulator transition in the bulk, so the mean-free path of a Josephson junction is expected to behave similarly.

D. Thouless length

We can define the Thouless length to be the thickness of the barrier region such that $E_{\mathrm{Th}}=k_BT$ at low enough T. Using this definition, shows that the Thouless length L_{Th} describes the thickness at which point transport crosses over from tunneling to incoherent thermally activated behavior at a given temperature.[15] The Thouless length will decrease with increasing T in the insulating regime, because the tunneling resistance is essentially independent of T, but the resistivity decreases dramatically with T due to its exponential activation; hence, the value of the resistance at the crossover decreases as the temperature increases, and this results in a smaller Thouless length (recall the tunneling resistance depends exponentially on the thickness of the barrier). Similarly, the Thouless length scale will increase as the Falicov-Kimball interaction increases. Here there is not as simple an argument to describe why this occurs, because both the tunneling resistance and the bulk resistivity increase with U^{FK}. But the tunneling resistance does not increase as rapidly (essentially because the barrier for tunneling is smaller than the excitation gap). This increase can be seen for the last two data points in Fig. 6.

It is more difficult to describe what the Thouless length is in a diffusive metal barrier. There is no crossover between tunneling and Ohmic transport, and the Thouless length decreases as a function of thickness here (see Fig. 6). This length scale appears to be more closely related (in a qualitative sense) to the mean-free path in the metallic regime. From a mathematical standpoint, the Thouless length describes the average distance that a thermal quasiparticle can diffuse through the barrier. One might expect that the resistance of the junction also has a sharp change as the thickness increases past the Thouless length in a diffusive metal barrier, but there is no indication of any such effect (see Fig. 4).

V. FRIEDEL-LIKE OSCILLATIONS

Since the pair-field amplitude has oscillatory behavior in addition to the exponential decay, we would like to see if one can make sense of the oscillations as arising from a Fermi-surface effect, as in the Friedel oscillations. Indeed, the fit of the data to a sinus-modulated form of Eq. (6) strongly suggests a wavelength of $2a$ (i.e., $2k=\pi/a$) for these oscillations independent of the value of U^{FK}. The amplitude of the oscillations increases with U^{FK}, and they cannot be determined by this fitting scheme for $U^{\mathrm{FK}}<4$. The amplitude of the oscillations decrease as the eighth power of distance from the interface. We believe the origin of these oscillations is the same as the Friedel oscillations in the DOS in the presence of an interface, i.e., a Fermi surface effect introduced by the sudden change of the scattering environment at the interface. Indeed, as U^{FK} is made larger, the barrier is more insulating, so the change of environment becomes more sudden; hence the amplitude of the oscillations increases. To illustrate this relation we calculated the local DOS at the Fermi energy $[N(\epsilon_F,x)]$ for a Josephson junction in the normal state (where the DOS is independent of T), the results for two values of U^{FK} in the barrier are shown in Fig. 7 ($U^{\mathrm{FK}}=0$ in the leads). The figure also shows the results of least-squares fits to a Friedel-oscillation form.

In the leads, the fit of the local DOS to a simple form $N(\epsilon_F,R)=a+b\sin(2k_FR+\phi)/(R+R_0)^p$ (where R is the distance from the interface) suggests values of $2k_F=\pi/a$ and $p=1$ in the leads. Phenomenologically, if we ignore scatterings inside the metal, we can model the interface between

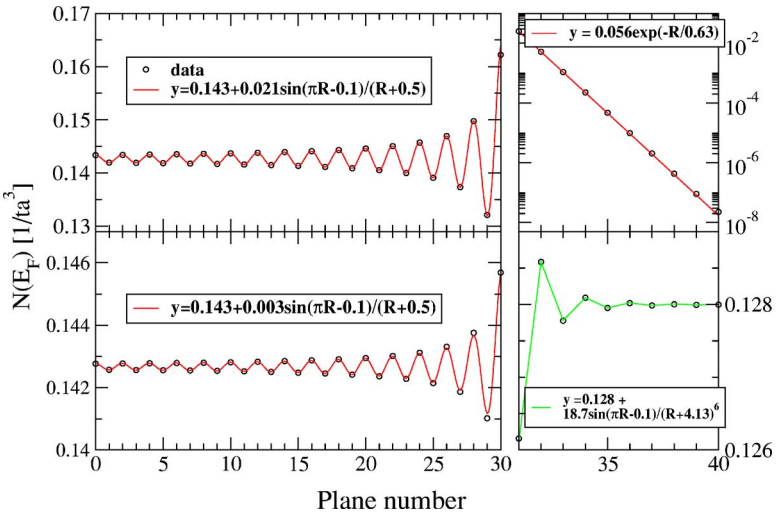

FIG. 7. (Color online) The DOS at Fermi energy for half of the junction (N is symmetric about 40.5 for the other half) at $T > T_c$. For clarity the scales are chosen to be different in the lead and barrier regions. Circles and lines represent the calculated data and the fit, respectively. In the barrier $U^{\mathrm{FK}}=2t$ for the lower half and $U^{\mathrm{FK}}=6t$ for the upper half. R stands for the distance from interface $|x-30.5|$.

two metals by a one-dimensional square well potential representing their work function mismatch (in contrast, in our microscopic model there is no chemical potential mismatch between the layers but the scattering strength changes at the interface). A simple single-particle quantum mechanical calculation then reveals that inside the metals both the DOS $N(\epsilon_F, R)$ and the electron number density $n(R)$ have Friedel oscillations with the same characteristic wave vector but an amplitude decay of $1/R$ and $1/R^3$, respectively (for the latter cf. Ref. 26). Note that in our multilayered nanostructures, the DOS has oscillations, but the charge does not; i.e., the simple quantum-mechanical calculations should be taken just as a qualitative guide to understand the full many-body system. Unfortunately, we have no simple way to explain the large power law observed in the case of the pair-field amplitude oscillations. We find it curious that the period of oscillation in the leads is two lattice spacings. This is what one would expect for a one-dimensional system, but not what one might expect for a three-dimensional system with a complicated Fermi surface.

In the barrier region, the fit again suggests that $2k_F = \pi/a$ independent of U^{FK}, but the decay exponent p increases with U^{FK} for diffusive barriers ($U^{\mathrm{FK}} < 5$) and the decay changes from a power-law to an exponential for larger values of U^{FK} as is apparent for $U^{\mathrm{FK}}=6$ in the top portion of the figure. When U^{FK} gets large enough, the oscillations decrease so rapidly, they become hard to see in the data anymore. Perhaps this occurs due to the small lifetime expected in an insulating barrier, which rapidly damps the oscillations out.

VI. CONCLUSIONS

In this work, we have applied the generalized concept of a Thouless energy to Josephson junctions with barriers that can be tuned through the metal-insulator transition. We found that in cases where the barrier is metallic and can be described by a diffusion constant (or equivalently by Ohm's law scaling), the quasiclassical approach works perfectly in describing the figure-of-merit even if the putative mean free path of the electrons drops well below a single lattice spacing. When the barrier is an insulator, a generalized version of the Thouless energy allows us to describe the figure-of-merit in a qualitatively similar fashion, although one can see differences from the quasiclassical predictions. We believe that this theoretical work shows that the generalized form of the Thouless energy is perhaps the most important single energy scale to describe transport in a Josephson junction, and we look forward to having experimentalists use it to describe their results. Some open questions about this part of our work are whether or not there is a universal form to the figure-of-merit versus Thouless energy curves when the barrier is an insulator, or whether different insulators fall on different curves. One might expect some form of universal behavior for thick enough barriers, because in that case the transport is also dominated by thermally excited diffusion.

We also were able to analyze Fermi-surface generated oscillations of different physical parameters (the DOS and the pair-field amplitude). The DOS behaves much like what one would expect from a standard Friedel-oscillation analysis when we are in the metallic leads, but the behavior is quite different in the barrier, especially when we pass through to the insulating side of the metal-insulator transition. In that case, the oscillations become undetectable, and the DOS decays exponentially at the chemical potential. The oscillations of the pair-field amplitude are even stranger. The power-law decay goes like the inverse eighth power of the distance from the interface (in the lead), which has no apparent explanation in terms of a simple Friedel-like analysis, although we believe their origin must come from Fermi-surface effects. Similarly, there does not appear to be any clear justification for why the period of the oscillations occurs at two lattice spacings.

Finally, we were able to analyze the decay of the superconducting parameters in the lead and in the barrier along conventional approaches, with the superconducting healing length in the leads agreeing with a Ginzburg-Landau type analysis, and with the decay length in the barrier agreeing with the conventional normal-metal coherence length and with the decay of the critical current as a function of barrier thickness.

ACKNOWLEDGMENTS

We are grateful to F. K. Wilhelm and T. T. Heikkilä for providing us with results of quasiclassical calculations and useful discussions. Support from ONR Grants No. N00014-99-1-0328 and No. N00014-05-1-0078 is acknowledged. Computer time was provided by the Arctic Region Supercomputer Center and the Mississippi Region Supercomputer Center (ERDC) through the HPCMP.

[1] J. T. Edwards and D. J. Thouless, J. Phys. C **5**, 807 (1972); D. J. Thouless, Phys. Rep., Phys. Lett. **13**, 93 (1974).
[2] A. Altland, Y. Gefen, and G. Montambaux, Phys. Rev. Lett. **76**, 1130 (1996).
[3] M. Janssen, *Fluctuations and Localization in Mesoscopic Electron Systems* (World Scientific, Singapore, 2001).
[4] Y. Alhassid, Rev. Mod. Phys. **72**, 895 (2000); I. L. Aleiner, P. W. Brouwer, and L. I. Glazman, Phys. Rep. **358**, 309 (2002).
[5] J. A. Melson, P. W. Brouwer, K. M. Frahm, and C. W. J. Beenakker, Europhys. Lett. **35**, 7 (1996); Ya. M. Blanter, A. D. Mirlin, and B. A. Muzykantskii, Phys. Rev. B **63**, 235315 (2001).
[6] T. Guhr, T. Wilke, and H. A. Weidenmüller, Phys. Rev. Lett. **85**, 2252 (2000).
[7] P. Dubos, H. Courtois, B. Pannetier, F. K. Wilhelm, A. D. Zaikin, and G. Schön, Phys. Rev. B **63**, 064502 (2001).
[8] For a review see B. Pannetier and H. Courtois, J. Low Temp. Phys. **118**, 599 (2000).
[9] T. M. Klapwijk, J. Supercond. **17**, 593 (2004).
[10] W. L. McMillan, Phys. Rev. **175**, 537 (1968); A. A. Golubov, F. K. Wilhelm, and A. D. Zaikin, Phys. Rev. B **55**, 1123 (1997).
[11] A. F. Volkov and H. Takayanagi, Phys. Rev. B **56**, 11184 (1997).
[12] G. Deutscher and P. G. De Gennes, in *Superconductivity*, edited by R. D. Parks (Marcel Dekker, New York, 1969).
[13] I. O. Kulik and A. N. Omel'yanchuk, J. Low Temp. Phys. **4**, 142 (1978).
[14] P. Dubos, H. Courtois, O. Buisson, and B. Pannetier, Phys. Rev. Lett. **87**, 206801 (2001).
[15] J. K. Freericks, Appl. Phys. Lett. **84**, 1383 (2004); Phys. Rev. B **70**, 195342 (2004); Phys. Status Solidi B **242**, 189 (2005).
[16] J. K. Freericks, A. N. Tahvildar-Zadeh, and B. K. Nikolić, IEEE Trans. Appl. Supercond. **15**, 896 (2005).
[17] P. Miller and J. K. Freericks, J. Phys.: Condens. Matter **13**, 3187 (2001); J. K. Freericks, B. K. Nikolić, and P. Miller, Phys. Rev. B **64**, 054511 (2001); **68**, 099901 (2003); Int. J. Mod. Phys. B **16**, 531 (2002).
[18] M. Potthoff and W. Nolting, Phys. Rev. B **59**, 2549 (1999).
[19] L. M. Falicov and J. C. Kimball, Phys. Rev. Lett. **22**, 997 (1969).
[20] J. K. Freericks and V. Zlatić, Rev. Mod. Phys. **75**, 1333 (2003).
[21] K. K. Likharev, Rev. Mod. Phys. **51**, 101 (1979).
[22] A. Khurana, Phys. Rev. Lett. **64**, 1990 (1990).
[23] D. Braun, E. Hofstetter, A. MacKinnon, and G. Montambaux, Phys. Rev. B **55**, 7557 (1997), and references therein.
[24] A. F. Ioffe and A. P. Regel, Prog. Semicond. **4**, 237 (1960).
[25] P. G. de Gennes, *Superconductivity of Metals and Alloys* (Perseus Books, Reading, MA, 1999); see also M. Tinkham, *Introduction to Superconductivity* (Dover, New York, 1996).
[26] A. Kiejna and K. F. Wojcienchowski, *Metal Surface Electron Physics* (Elsevier Science, Amsterdam, The Netherlands, 1996).